Structural studies of Bi_2O_3-Nb_2O_5-TeO_2 glasses: evaluation of metastable "anti-glass" crystallization behavior and potential polyamorphism leading to new nanocomposite materials

Martin C. Wilding[1 *], Gaelle Delaizir[2], Chris J. Benmore[3], Yann Gueguen[4], Morgane Dolhen[2], Jean-René Duclère[2], Sébastien Chenu[2], Sohei Sukenaga[5], Paul F. McMillan[6 *]

[1] Department of Physics, University of Bath, Claverton Down, Bath BA4 7AY, UK

[2] Université Limoges, CNRS, ENSCI, Science des Procédés Céramiques et de Traitements de Surface (SPCTS), UMR 7315, Centre Européen de la Céramique, 87068 Limoges, France

[3] X-ray Science Division, Argonne National Laboratory, Argonne IL 60439 USA

[4] Institut de Physique de Rennes, UMR CNRS 6251, Département Mécanique et Verre, Université Rennes 1, France

[5] Institute of Multidisciplinary Research for Advanced Materials (IMRAM), Tohoku University, 2-1-1, Katahira, Aoba-ku, Sendai 9808577 Japan

[6] Christopher Ingold Laboratory, Department of Chemistry, University College London, 20 Gordon Street, London WC1H 0AJ, UK

* Corresponding authors: mw927@bath.ac.uk ; p.f.mcmillan@ucl.ac.uk

Abstract

Bi_2O_3-Nb_2O_5-TeO_2 glasses show unusual annealing behavior with appearance of spherulites within the matrix glass structure for the $Bi_{0.5}Nb_{0.5}Te_3O_8$ composition. The textures resemble those found previously among polyamorphic Al_2O_3-Y_2O_3 glasses containing metastably co-existing high- and low-density phases produced during quenching. However the spherulites produced within the Bi_2O_3-Nb_2O_5-TeO_2 glass are crystalline and can be identified as an "anti-glass" phase related to β-$Bi_2Te_4O_{11}$. We used high energy synchrotron X-ray diffraction data to study structures of binary and ternary glasses quenched from liquids within the Bi_2O_3-Nb_2O_5-TeO_2 system. These reveal a glassy network based on interconnected TeO_4 and TeO_3 units that is related to TeO_2 crystalline materials but with larger Te...Te separations due to the presence of TeO_3 groups and non-bridging oxygens linked to modifier (Bi^{3+}, Nb^{5+}) cations. Analysis of the viscosity-temperature relations indicates that the glass-forming liquids are "fragile" and there no evidence for a LLPT occurring in the supercooled liquid. The glasses obtained by quenching likely correspond to a high-density amorphous (HDA) state. Subsequent annealing above T_g shows mainly evidence for crystallization of the "anti-glass" tellurite phase. However, some evidence may exist for simultaneous formation of nanoscale amorphous spherultites that could correspond to the LDA polyamorph. The quenching and annealing behavior of Bi_2O_3-Nb_2O_5-TeO_2 supercooled liquids and glasses is compared with similar materials in the Al_2O_3-Y_2O_3 system.

1. Introduction

The phenomenon of "polyamorphism" recorded among ceramic glass-forming liquids and the amorphous solids derived from them is receiving increasing attention as a potential route to producing new classes of nano- to microscale composite materials. It can be implemented alongside metastable crystallization by annealing or synthesis schedules used to achieve ceramic-matrix composites (CMCs) with controllable mechanical, thermal and other properties. The concept of polyamorphism recognizes the existence of different forms of a given amorphous substance with substantial variations in their local structure and physical properties. Different polyamorphs of a given glassy material or another type of amorphous solid can be produced by varying the synthesis route, or by subjecting the material to intense radiation or physical stresses including high pressure. In some cases, an abrupt transformation between polyamorphic forms with different densities has been recorded upon subjecting the glass to high mechanical stresses,that resembles a first order phase transition in crystalline solids. Density driven phase transitions have also been observed among liquids as a function of the pressure or temperature, and one or other of the glassy polyamorphs can be recovered by quenching at different rates. That was the case described for a range of compositions with between approximately 20-35 mole% Y_2O_3 in the Al_2O_3- Y_2O_3 (AY) system[1-5]. Those results provided first evidence for the existence of liquid-liquid phase transitions (LLPT) occurring at constant chemical composition, that had been predicted theoretically on thermodynamic grounds[6,7]. Such LLPT are now thought to occur among a wide range of liquid systems[7].

During initial quenching experiments Aasland and McMillan observed that "spherulites" of a different phase appeared spontaneously and grew within the supercooled liquids[1]. The spherulites were identified as mainly glassy in nature, and their chemical compositions were found to be indistinguishable both from the initial bulk liquid and the surrounding glassy matrix formed upon quenching to ambient conditions. The result was interpreted as due to a LLPT occurring between high- and low-density liquid (HDL, LDL) phases in the supercooled state that was arrested during the quench to provide metastably coexisting low- and high-density polyamorphs (LDA, HDA). In further series of quenching experiments, Wilding et al prepared new samples that exhibited different curvilinear textures separating different amounts of the LDA and HDA polyamorphs. Calorimetry studies could establish that the two glassy forms had different glass transition (T_g) values, as well as a value of ~30 kJ/mol for the enthalpy of the transition between them. The glassy structures were studied using X-ray and neutron scattering, as well as microbeam Raman spectroscopy[3,4]. The spherulites were shown to have ~4% lower density than the surrounding glassy matrix[5]. The calorimetric data permitted a prediction of the viscosity-temperature relationships in the stable and supercooled liquid states that led to a description of the LDL phase as less "fragile" with more Arrhenian relaxation properties than HDL.

In pioneering experiments using X-ray scattering combined with containerless levitation techniques, N. Greaves and co-workers showed that the LLPT gave rise to unusual periodic thermal fluctuations[8,9]. However, although these results and their interpretation were questioned initially, the LLPT interpretation appears to be validated by careful analysis of the data [8,10]. The occurrence of a LLPT in the supercooled liquid is also supported by polarizable ion (PI) MD simulations, that exhibit random but persistent fluctuations between low- and high-density states of the supercooled liquid as the critical temperature is approached[11].

In the case of the glassy polyamorphs, some authors have also questioned the glassy nature of the LDA material, mainly by observing that crystalline peaks are observed in microbeam X-ray diffraction studies[12]. In fact Aasland and McMillan already noted the crystalline aspect of certain spherulites obtained during their quench study of AY liquids, and crystalline Bragg peaks were present in diffraction data for samples containing a large fraction of the LDA polyamorph[1] (Fig. 1). In samples prepared for a Raman spectroscopic study using a quench technique that led to large regions of the LDA and HDA polyamorphs separated by curvilinear boundaries[4], crystals were clearly observed growing away from certain parts of the LDA-HDA interface into the LDA phase (Fig. 1). It is clear that metastable crystallization can and often does compete with the LLPT or polyamorphic HDA/LDA transitions, either during the initial cooling event or following annealing of the quenched glasses. That is an important feature leading to the possible development of novel classes of hierarchical CMC materials.

The observations and discussions concerning polyamorphism in Y_2O_3-Al_2O_3 materials are now linked to new phenomena observed among glasses within the Bi_2O_3-Nb_2O_5-TeO_2 system [13,14]. In this case, partially ordered crystalline materials have been described in terms of the "anti-glass" model introduced by Burckhardt, Trömel and co-workers[15] for tellurite systems with fluorite-related structures [14]. In this case, a metal sublattice based on large cations such as Sr^{2+}, Pb^{2+}, Ln^{3+} (Ln = Y, lanthanide ions) along with Te^{4+} form an ordered array that gives rise to crystalline Bragg peaks in X-ray diffraction experiments, but the anion positions can be disordered, and both sites might be incompletely filled. A similar situation occurs for cubic ZrO_2 stabilized by substitution of Y^{3+} on some cation positions along with vacancies present on the O^{2-} sites. Such materials typically exhibit crystalline X-ray diffraction patterns due to the heavy atoms, but can appear amorphous to Raman and IR spectroscopy due to the inability of phonons to propagate through the anion-deficient lattice[16]. Similar sublattice disordering occurs in systems including AgI, PbBr, LaF, fluorite- and more complex-structured materials that are known to be solid electrolytes and (super)ionic conductors.

Bertrand et al described Bi_2O_3-Nb_2O_5-TeO_2 glasses produced by melt quenching. Upon annealing, a sample with composition $Bi_{0.5}Nb_{0.5}Te_3O_8$ developed spherulitic structures that appeared to be analogous to the initial LDA-HDA polyamorphic textures observed by Aasland and McMillan for polyamorphic AY glasses[13](Fig. 1). However, although the compositions of the Bi_2O_3-Nb_2O_5-TeO_2 spherulites obtained by Bertrand et al. remained identical to those of the surrounding matrix glass, optical and scanning electron microscopy results along with X-ray diffraction indicated that they were fully crystalline. Bertrand et al. interpreted their results in terms of the "anti-glass" model of Trömel et al. that had already been suggested for tellurite systems[13].

Crystalline $Bi_{0.5}Nb_{0.5}Te_3O_8$ has a cubic structure related to $TiTe_3O_8$. Other "anti-glass" materials in the Bi_2O_3-Nb_2O_5-TeO_2 system include β-$Bi_2Te_4O_{11}$ with a fluorite-related arrangement of Bi^{3+} and Te^{4+} cations occupying 1/3 and 2/3 of the cation sites, respectively, and O^{2-} vacancies occurring on 1/12 of the anion sites[17]. Bertrand et al. proposed that the quenched matrix glass was fully structurally disordered, but the spherulites that appeared had an "anti-glass" structure containing positional ordering of the metal cations on the fluorite lattice as demonstrated by Raman experiments[13]. However, further investigations by TEM have indicated that some of the nanometer-sized spherulites that appeared might be amorphous. Those analyses are continuing and will be reported elsewhere (G. Delaizir et al., in prep).

In the present work we obtained high energy synchrotron X-ray diffraction (HE-XRD) data for fully glassy and partially recrystallized samples along the TeO_2-Bi_2O_3 and TeO_2-Nb_2O_5 joins and within the Bi2O3-Nb_2O_5-TeO_2 system. The data provide new constraints on the local structural arrangements

within the matrix glasses relative to the "anti-glass" crystallization features and events observed within the system.

2. Experimental

High energy X-ray diffraction (HE-XRD) data were obtained over a wide *Q* range for three series of tellurite glasses. TeO_2-Bi_2O_3, TeO_2-Nb_2O_5 and TeO_2-Bi_2O_3-Nb_2O_5 samples were prepared from mixtures of high purity TeO_2, Bi_2O_3 and Nb_2O_5 powders melted at 850°C in Pt crucibles and quenched by dipping the bottom of the crucible in water. Along the TeO_2-Bi_2O_3 binary, glasses containing no distinguishable crystalline Bragg peaks could only be prepared very close to the TeO_2 composition (98 mole% TeO_2). Glass formation extended further along the TeO_2-Nb_2O_5 binary, up to 20 mole% Nb_2O_5. All of the ternary compositions studied here appeared to be fully glassy. HE-XRD measurements were performed at the Advanced Photon Source (APS) at Argonne National Laboratory (USA) using the high energy beamline 6-ID-C. Using high energy X-rays (100.131 keV, corresponding to λ=0.123822Å) allows data collection to high values of the scattering vector (*Q*) with minimal corrections for absorption and multiple scattering. The incident beam was collimated to 0.25 x 0.5 mm. Scattered XRD patterns were collected using a Perkin Elmer model 1621 detector mounted vertically on a platform that could be moved along the beam axis to select the distance between the sample and the active areas of the detector. For these measurements the detector was typically set at ~45 cm from the sample. The sample-detector distance, coordinates of the direct beam and the angles of tilt and rotation were refined by calibration against a crystalline CeO_2 standard. The detector had a 41 cm^2 active area using an a-Si active surface with spatial resolution 200 µm.

A 1D diffraction pattern was obtained by integrating over all the pixels using Fit2D[18]. To maximize the value of scattering vector the detector was offset with the beam stop forming one corner of the area detector and a cake extracted to eliminate unresponsive pixels along the detector edge. Diffraction data were obtained up to Q=22Å^{-1} with an instrumental resolution $\Delta Q/Q$ = 0.5%. Following background subtraction the total X-ray structure factor was obtained using PDFgetX2[19] as:

$$S(Q) = \frac{[I(Q) - C(Q) - \sum_i f_i^2(Q)]}{[\sum_i f_i(Q)]^2}$$

Here I(Q) is the corrected initial scattered intensity, C(Q) is the Compton scattering contribution and f_i(Q) the set of X-ray (electronic) form-factors[20]. In Bi_2O_3-bearing samples the scattering intensity also contained fluorescence contributions that were accounted for by subtracting a constant value from I(Q).

Results are reported first as reciprocal space correlations of the total scattering (*S(Q)*) that represents the weighted sum of partial structure factors, expressed using the Faber-Ziman formalism[21] . The sine Fourier transform of the total, multi-component structure factor provides the total (pseudo-nuclear) pair distribution function, G(r).

$$G(r) - 1 = \frac{1}{2\pi^2 r\rho}\int_{Qmin}^{Qmax} Q[S(Q) - 1]\sin(Qr)\,dQ$$

Here Q_{max} and Q_{min} represent the upper and lower limits of the finite range in reciprocal space studied and ρ is the atomic number density[21]. The G(r) function emphasizes local structure. For glassy materials it is convenient to express the pair distribution function in terms of the total correlation function, T(r), or the differential distribution function (D(r)), that are used to highlight longer distance correlations. These are defined by:

$$D(r) = 4\pi r\rho[G(r)] - 1$$

$$T(r) = 4\pi r\rho[G(r)]\ .$$

Viscosity measurements in the glass transition range were made using the indentation method on a home-made apparatus[22]. The indenter used was a 2 mm diameter SiC sphere. The viscosities of the sample melt were measured using the rotating cylinder method. The information on the viscometer has been already reported in detail previously[23]. The sample was placed in a Au crucible and heated up to 1113 K (840 °C) in air. The lower limit of the examined temperature was set as 1033 K (760 °C) in order to avoid sample crystallization. The inner cylinder (i.e. Pt-20mass%Rh bob) was immersed 10 mm from the melt surface. The Au crucible was then rotated at 70 rpm in order to collect the electrical voltage attributable to the torque on the inner cylinder. The measurement was performed during cooling of the melt for temperatures that changed in steps of 20 K. At the each examined temperatures, the test sample was melted until the detected voltage (i.e. viscosity) became constant. The viscosity of the test sample was measured three times at each examined temperatures the errors in the electric voltage were within ±3%.

3. Results

Diffraction data obtained for TeO_2-Bi_2O_3 samples are shown in Figure 2. Only the sample containing 2 mole% Bi_2O_3 was fully glassy whereas the other patterns were dominated by Bragg diffraction peaks from crystalline TeO_2 and β-$BiTi_5O_{11}$. The latter phase lies at the origin of the "anti-glass" model of Trömel et al that was applied by Bertrand et al to understand crystallization effects among the spherulites that appeared during annealing in the ternary Bi_2O_3-Nb_2O_5-TeO_2 system[24]. Here we focus our analysis on the fully glassy materials at high TeO_2 content that we used to model the structural features present within a hypothetical pure TeO_2 glass.

The total structure factor for the 98% TeO_2 sample shows prominent features that persist to the highest *Q* studied here (28.5 $Å^{-1}$). A first strong peak in the diffraction pattern occurs at 2 $Å^{-1}$. This principal peak[25] can be associated with spatial correlations over medium range length scales and often reflects the chemical ordering of different species[26]. In the TeO_2-Bi_2O_3-Nb_2O_5 samples studied here the peak can be identified it with Te...Te correlations occurring with real space periodicity ~3-4 Å. Detailed structural assignments of the features in S(Q) and D(r) are discussed below.

The higher Q oscillations in S(Q) reveal short range order occurring within the main glass-forming structural units. Fourier transformation leads to the real space function D(r) that reveals characteristic distances within the glass structure. Faber-Ziman weightings associated with the different pair correlations are given in Table 1, these are evaluated at Q=0 since there is a Q-dependence to the form factors. These indicate the relative contributions of each atom pair and they show that main contributions occur from Te-O and Te...Te correlations, as expected. The first main peak in D(r) occurs at 1.91 Å and is due to Te-O distances within a glass matrix dominated by TeO_3 and TeO_4 units, consistent with bond valence parameter predictions[27,28] (Fig. 3). This interpretation is supported by Raman spectroscopic results for tellurite glasses[29]. The second peak at 3.5 Å is mainly due to Te...Te correlations within the second coordination shell around the network-forming cations, and it gives rise to the principal peak at 2 $Å^{-1}$ in S(Q). The peak in D(r) has an obvious shoulder towards longer r that might initially suggest the presence of different populations of TeO_n polyhedra. Further analysis of the glass diffraction data has been made using reverse Monte Carlo (RMC) modelling. An RMC model was constructed assuming a pure TeO_2 glass composition. A 3000 atom configuration generated with cut-off constraints similar to McLaughlin[30,31] was used to establish the partial Te-Te, Te-O and O-O contributions to S(Q) and D(r) (Fig 3). The RMC simulations demonstrate that the asymmetric peak

at 3.5 A in the D(r) comprises overlapping Te-Te and Te-O partial contributions. The Te-Te correlation is asymmetric in real space and the resulting configurations indicate that the glass is a mixture of both 3- and 4- coordinate Te-O polyhedra that can be both corner- and edge-shared. This modelled glass structure is the most disordered structure consistent with the data and yields a structure considerably more disordered than the relatively open-structured face- or corner-shared structures of the TeO2 crystalline polymorphs[32].

Table 1 : Faber-Ziman weightings (at Q=0) for TeO_2-Bi_2O_3-Nb_2O_5 glasses

(a) TeO_2-Bi_2O_3 and TeO_2-Nb_2O_5 compositions

TeO2-Bi2O3	98% TeO2		TeO2-Nb2O5	98% TeO2	95% TeO2	90% TeO2	85% TeO2	80% TeO2
Te-Te	0.51		Te-Te	0.54	0.49	0.40	0.34	0.27
Te-O	0.34		Te-O	0.35	0.34	0.32	0.30	0.27
Te-Bi	0.07		Te-Nb	0.04	0.08	0.15	0.19	0.23
Bi-Bi	0.00		Nb-Nb	0.00	0.00	0.01	0.03	0.05
Bi-O	0.02		Nb-O	0.01	0.03	0.06	0.08	0.11
O-O	0.05		O-O	0.05	0.06	0.06	0.07	0.07

(b) Ternary TeO_2-Bi_2O_3-Nb_2O_5 glasses

	95% TeO2	90% TeO2	85% TeO2	80% TeO2	75% TeO2	70% TeO2
Te-Te	0.47	0.37	0.29	0.24	0.19	0.19
Te-O	0.32	0.27	0.25	0.21	0.19	0.19
Te-Nb	0.04	0.07	0.08	0.09	0.09	0.10
Te-Bi	0.08	0.13	0.17	0.18	0.20	0.20
Nb-Nb	0.00	0.00	0.01	0.01	0.01	0.01
Nb-O	0.01	0.02	0.03	0.04	0.05	0.05
Nb-Bi	0.00	0.01	0.02	0.04	0.05	0.05
Bi-Bi	0.00	0.01	0.02	0.04	0.05	0.05
Bi-O	0.03	0.05	0.07	0.09	0.10	0.10
O-O	0.05	0.05	0.05	0.05	0.05	0.05

Within the TeO_2-Nb_2O_5 system glasses are produced readily at up to 20 mole% Nb_2O_5 composition (Fig. 4). Analysis of S(Q) and D(r) data for the 98% TeO_2 (Te98Nb2) composition reveals very similar structural features to the 98 mol% glass produced along the TeO_2-Bi_2O_3 binary. However as as the Nb_2O_5 concentration is raised there are changes in the S(Q)) appear with reflect the increased partial contributions of Te-Nb and to a lesser extent Nb-O correlations to the total structure factor at it's transform (Table 1).

We observe a slight decrease in the height of the first peak in the diffraction pattern that shifts to lower Q as Nb_2O_5 increases (Fig. 4a) and corresponding increases in intensity at higher Q. The pair distribution function, shown as the D(r) in figure 3b also shows continuous changes in the underlying structure as Nb_2O_5 is added. The first peak at 1.92 Å increases in intensity as Nb_2O_5 is added. The radial distances for 4-6 coordinate NbO_n polyhedra are 1.83 to 1.98 Å for 4-6 coordinate NbO_n polyhedra based on tabulated bond-valance values[27] and the intensity changes are consistent with the increasing contribution of an approximately Gaussian Nb-O correlation at 1.89 Å. This suggested mixture of 4 and 6 coordinate Nb-O overlaps with the Te-O correlations and the contributions cannot be distinguished

by these diffraction experiments. The increase in intensity of the first peak and at higher radial distance as Nb_2O_5 is added, reflects the increased contribution of Nb-atom pairs. Even in the most Nb_2O_5-rich compositions the diffraction data are dominated by Te-O and Te-Te. Preliminary RMC configurations suggest that the partial contribution from Te-Nb has a first peak that is broader and more asymmetric than Te-Te and has oscillations in Q are out of phase with the Te-Te partial contribution. This is consistent with the decrease in the intensity of the first peak in the S(Q) (Fig 4a) and shift to slightly higher r of the peak at 3.5 Å in real space (Fig 4b) as Nb_2O_5 is added.

In the ternary TeO_2-Bi_2O_3-Nb_2O_5 system the glass-forming range is extended further to 70% TeO_2. Once more, the structural data show a similar persistence of the underlying TeO_2 framework based on mixed TeO_3 and TeO_4 structural units (Fig 5). In this case there is a progressive increase in the first peak in the diffraction pattern at 1.98 $Å^{-1}$. This suggests that the partial contributions of the Te-Te and Te-Bi to the S(Q) are similar. At higher Q there is a change in the intensity of the peak at at 3.6 $Å^{-1}$and decrease in the intensity of the high Q shoulder to this feature as the Bi_2O_3 and Nb_2O_5 concentrations increase. In the real space transform the most Te-rich glass is structurally similar to the 98% TeO_2 compositions in the Bi_2O_3- and Nb_2O_5-TeO_2 binary compositions and as expected from the Faber-Ziman weightings (Table 1) the main correlations are Te-O and Te-Te. As the TeO_2 content is reduced and the Bi_2O_3 and Nb_2O_5 jointly increases the peak at 1.9 Å shows a decrease in intensity, as outlined above this will have overlapping contributions from Te-O and Nb-O correlations in 3- and 4-coordination and 4- and 6-coordination by oxygen. In these compositions the weightings are such that Bi-pair contributions will increases as concentrations change and this is reflected in the changes in height of the peak at ~2.25 Å. Again bond-valance calculations give the radial distance for 4- and 6-coordinated BiO_n units of 2.19 to 2.35 Å respectively and suggest a mixture of these coordination polyhedra that contribute to the peak at 2.25 A. The correlations at higher r shift to grater radial distance and represent overlapping partial radial distributions functions of all partials with the greatest contribution from Te-Te, Te-Bi, Te-Nb and Te-O, the latter contributing to the high-r shoulder. These cannot be resolved and RMC fits have not been attempted. The progressive changes in both S(Q) and D(r) with composition do not show any abrupt changes in structure and indicate that the main structure changes reflect a difference in the relative contributions of the scattering atom pairs and progressive modification of the underlying disordered TeO_2-glass structure with addition of BiO_n and NbO_n polyhedra units.

Discussion

Pure TeO_2 is a poor glass former but glasses are formed readily with even small amounts of modifier components including metal oxides or fluorides. The local coordination environments around the Te^{4+} cations are readily understood in terms of VSEPR (valence shell electron pair repulsion) models. The crystalline polymorphs of TeO_2 contain TeO_4 polyhedra that are based on trigonal bipyramidal structures (TeO_4E) with an electron lone pair (E) occupying an equatorial position, and in which two of the oxygen atoms are corner- or edge-linked between adjacent polyhedra[32]. The presence of the lone pair gives rise to useful non-linear optical properties. The oxygen atoms involved in bridging between TeO_4 units occur at axial and equatorial positions[31,33] . Adding modifier components to provide glass-forming compositions causes disruption of the network with the appearance of TeO_3^{2-} units containing non-bridging oxygens that are coordinated to the modifier cations[34]. The TeO_3^{2-} groups adopt a distorted tetrahedral geometry with the lone pair forming one apex. IR and Raman investigations of Nb^{5+}- and Bi^{3+}-bearing tellurite glasses indicate that they contain chains of corner-linked TeO_3 and TeO_4 units with non-bridging oxygens coordinating NbO_6 and BiO_6 units[29].

Our HEXRD studies of these glass structures are consistent with these findings. The similarity of the S(Q) patterns indicate that the overall TeO_2 framework is only slightly perturbed by the addition of the

modifier component, and structural correlations persist over a wide Q range. The first dominant peak in S(Q) is associated with Te...Te correlations occurring at around 3.5 Å that corresponds to the Te...Te distances in Na_2TeO_3 and $Na_2Te_4O_9$ [31,33], but is longer than those found in crystalline TeO2 polymorphs[32]. That indicates that the addition of even small amounts of either Nb_2O_5 or Bi_2O_3 as modifier components causes the structure to relax internally while maintaining the highly ordered arrangement of the Te^{4+} cations. The improvement in glass forming ability thus likely results from the increased entropy associated with the linkage disorder caused by the random distribution of TeO_4 and TeO_3 units, along with the equatorial *vs* axial positions of the bridging *vs* non-bridging O^{2-} species. That finding immediately lends itself to the "anti-glass" model used to describe metastable crystallization features in Bi_2O_3-Nb_2O_5-TeO_2 glasses[13].

We now examine the structural relaxation properties of the glass-forming liquids. Viscosity (η) measurements made near the glass transition for the $Bi_{0.5}Nb_{0.5}Te_3O_8$ glass exhibits a steep activation energy for viscous flow. These can be compared with viscosity data for the higher temperature liquid and for liquid TeO_2 [35] that show a much lower activation energy. Combining the two data sets results in a log η - 1/T plot that can be fitted to a single Volger-Fulcher-Tamman (VFT) relation (Fig. 6). The VFT fit is strongly curved indicating a highly non-Arrhenian or "fragile" nature for the stable and supercooled tellurite liquids[36]. The fragility index (m) is obtained by considering the apparent activation energy (ΔH^*), obtained from the initial slope of the viscosity-temperature relation in the vicinity of the glass transition ($m=-\Delta H^*/RT_g$). Classic, “strong” liquids such as silica have a fragility index of 20, while moderately strong liquids such as sodium silicates have a fragility index of ~85. The estimated value for these tellurite compositions is 78. The fragility indices determined for some of the most fragile liquid systems, such as ZBLAN20 and Ca-K-nitrate (176 and 210 respectively)[37] the high-density liquid (HDL) phase of Al_2O_3-Y_2O_3 giving rise to HDA glassy polyamorphs also has a high fragility. This analysis is consistent with previous estimates of the fragility of sodium tellurite liquids[37]. Our impetration of the viscosity-temperature data for the tellurite liquids is that they result in a high density amorphous (HDA) polyamorph upon quenching, with no indication of any structural or thermodynamic transition in the supercooled state that might be associated with transformation to a low-density (LDL) liquid. That behavior is different to that observed for supercooled liquids in the Al_2O_3-Y_2O_3 system[5].

During annealing the $Bi_{0.5}Nb_{0.5}Te_3O_8$ glass showed appearance of spherulitic structures that were mainly identified with "anti-glass" crystalline structures[17]. However, a very few of the spherulites remained glassy. These changes occurred as the initial HDA glasses were heated above their glass transition temperature (T_g^{HDA}) and crystallization into the "anti-glass" phase might have occurred directly. However, the presence of some amorphous spherulites on a nanometric scale could indicate that a possible transformation into a low-density (LDA) glassy polyamorph might have occurred simultaneously, in competition with the recrystallization event. Interestingly, no spherulites developed for the $12.5Bi_2O_3$-$12.5Nb_2O_5$-$75TeO_2$ composition upon annealing.

The behavior can be compared with that found for the Al_2O_3-Y_2O_3 supercooled liquids and glassy materials. In that case the LLPT transition temperature occurred in the supercooled liquid range slightly above the glass transition (T_g^{HDA}) for the supercooled HDL phase, but could not be completed during the quench experiments. In addition, emergence of crystalline material based on a disordered AY_{ss} garnet structure was observed both during initial quenching and subsequent annealing of the HDA-LDA glassy composite materials. In that case it was interesting that the crystalline material was produced within the LDA phase (Fig. 1). In the case of TeO_2-Bi_2O_3-Nb_2O_5 glasses, it is not yet clear if the anti-glass crystals formed are structurally related to the potential LDA spherulites appearing within the system upon annealing. That will require further investigation.

For the $Bi_{0.5}Nb_{0.5}Te_3O_8$ glass composition the differential scanning calorimetry (DSC) results showed a glass transition (T_g) at 350°C[13]. This was followed by an exothermic peak near 400°C that was associated with crystallization of the anti-glass phase. There was no evidence for a subsidiary exotherm that might be interpreted as due to a LLPT between the HDL supercooled liquid phase and an LDA polyamorph, as was observed previously for Al_2O_3-Y_2O_3 liquids during re-heating the metastably quenched HDA glass[38]. That could mean that the recrystallization and potential HDL-LDA transformation events occur in competition with each other in the Bi_2O_3-Nb_2O_5-TeO_2 system, over a similar range of temperatures and annealing timescales.

Conclusions

Our HEXRD data for binary and ternary glasses in the Bi_2O_3-Nb_2O_5-TeO_2 system reveal a glassy network based on interconnected TeO_4 and TeO_3 units that appears to remain relatively unchanged from the parent TeO_2 system. The diffraction data are dominated by Te...Te correlations at distances greater than those found in pure TeO_2 phases but correspond to those for crystalline tellurites containign modifier cations. Analysis of the viscosity-temperature relations shows that the glass-forming liquids are highly "fragile" in nature. There no evidence for a LLPT occurring during cooling, and the glasses obtained by quenching likely correspond to a high-density amorphous (HDA) state. During subsequent annealing above T_g, X-ray diffraction, SEM and Raman spectroscopy data indicate crystallization of an "anti-glass" tellurite phase based on β-$Bi_2Te_4O_{11}$. Formation of this compound from the glassy material requires only small adjustments in the cation positions, sufficient to achieve an ordered array that results in positional (but not chemical) order and crystalline diffraction while the Raman spectra continue to exhibit broad "amorphous" signatures[13,16]. It is possible that some nanoscopic spherulites appearing initially upon annealing are amorphous and that these could constitute examples of an LDA material produced simultaneously *via* a polyamorphic transformation occurring simultaneously with the anti-glass recrystallization event. The behavior can be compared and contrasted with that reported previously for Al_2O_3-Y_2O_3 glasses and glass-forming liquids. In that case the LLPT is sampled during supercooling but is not fully achieved during quenching to result in mixed HDA-LDA glasses. A metastable transition then occurs during re-heating above T_g for the HDA polyamorph, with appearance of the LDA phase below its glass transition[38]. However, both the initial quenching event and subsequent annealing result in simultaneous nucleation of a crystalline Al_2O_3-Y_2O_3 solid solution phase. Our conclusion is that the transformations occurring within the Bi_2O_3-Nb_2O_5-TeO_2 system might be analogous to those observed among Al_2O_3-Y_2O_3 and other rare earth (RE) oxide supercooled liquids, glasses and metastable crystalline phases, but with subtle but important differences in the relative temperatures and timescales over which they occur. Most importantly, the combination of metastable crystallization and polyamorphic transformation events provides a new routes to creating new families of nanocomposite materials with useful properties.

Acknowledgements

We would like to thank Professor Alex Navrotsky for discussion. The HEXRD work is supported by the US DOE Argonne National Laboratory under contract number DE-AC02-06CH11357. We would like to sincerely thank Prof. Kunihiko Nakashima (Kyushu University) and Prof. Noritaka Saito (Kyushu University) for supporting us on the viscosity measurements PFM acknowledges support from the EPSRC.

FIGURE CAPTIONS:

Figure 1. Spherulites grown in $Bi_{0.5}Nb_{0.5}Te3O_8$ glass matrix when heated to 380°C. The two images for the tellurite glasses show formation of “anti-glass” spherulites at 4 (a) and 11hour (B)[13]. The

development of cracks in the spherulites indicates confined growth and differs from the congruent crystallisation characteristic of the vitrification process. The similar textures developed in yttrium aluminate glasses are shown from the paper by Aasland and McMillan[1] (c) and more recent publications (d).

Figure 3. The total structure factor for Bi_2O_3-TeO_2 glasses, S(Q), obtained by HEXRD at sector 6 (6-ID-D), APS. Three compositions are shown (A), those with 80 and 85% TeO_2 show Bragg peaks consistent with the presence of TeO_2 and the anti-glass β-$Bi_2Te_4O_{11}$. The partial structure factors $S_{\alpha\beta}(Q)$ are shown for the 98% TeO_2 glass(B) from the RMC fit (assuming this structure is a pure TeO_2 glass). The partial contributions in real space, $g_{\alpha\beta}(r)$ are also shown (C).

Figure 4. The total structure factors for Nb_2O_5-TeO_2 glasses, obtained from HEXRD data, these are shown displaced for clarity (A). The real space transforms (As D(r)) are also shown (B)

Figure 5. The HEXRD S(Q) for NB_2O_5-Bi_2O_3-TeO_2 glasses, also displaced for clarity(A) and the real space transform, as D(r) B.

Figure 6. High and low-temperature viscosity data for $Bi_{0.5}Nb_{0.5}Te_3O_8$ composition liquids (corresponding to 85% in this work) compared with rotating cylinder viscosity data for pure TeO_2 (Veber and Mangin, 2008). A Volger-Fulcher-Tamman (VFT) fit is also shown.

REFERENCES

1 S. Aasland and P. F. McMillan, Nature **369** (6482), 633 (1994).

2 P. F. McMillan, C. Ho, S. Aasland, A. YeganehHaeri, and R. Weber, in *Structure and Dynamics of Glasses and Glass Formers*, edited by C. A. Angell, K. L. Ngai, J. Kieffer et al. (1997), Vol. 455, pp. 377; P. F. McMillan, M. Wilson, and M. C. Wilding, Journal of Physics-Condensed Matter **15** (36), 6105 (2003).

3 M. C. Wilding, M. Wilson, C. J. Benmore, J. K. R. Weber, and P. F. McMillan, Physical Chemistry Chemical Physics **15** (22), 8589 (2013).

4 M. C. Wilding, M. Wilson, P. F. McMillan, T. Deschamps, and B. Champagnon, Physical Chemistry Chemical Physics **16** (40), 22083 (2014).

5 M. C. Wilding, M. Wilson, P. F. McMillan, C. J. Benmore, J. K. R. Weber, T. Deschamps, and B. Champagnon, Journal of Non-Crystalline Solids **407**, 228 (2015).

6 E. Rapoport, Journal of Chemical Physics **46** (8), 2891 (1967); E. Rapoport, Journal of Chemical Physics **48** (4), 1433 (1968); I. L. Aptekar and Ponyatov.Yg, Physics of Metals and Metallography-Ussr **25** (5), 10 (1968).

7 D. Machon, F. Meersman, M. C. Wilding, M. Wilson, and P. F. McMillan, Progress in Materials Science **61**, 216 (2014); P. F. McMillan, G. N. Greaves, M. Wilson, M. C. Wilding, and D. Daisenberger, in *Liquid Polymorphism*, edited by H. E. Stanley (2013), Vol. 152, pp. 309.

8 G. N. Greaves, M. C. Wilding, S. Fearn, D. Langstaff, F. Kargl, S. Cox, Q. V. Van, O. Majerus, C. J. Benmore, R. Weber, C. M. Martin, and L. Hennet, Science **322** (5901), 566 (2008).

9 G. N. Greaves, M. C. Wilding, F. Kargl, L. Hennet, and O. Majerus, in *Glass - the Challenge for the 21st Century*, edited by M. Liska, D. Galusek, R. Klement et al. (2008), Vol. 39-40, pp. 3; G. N. Greaves, M. C. Wilding, Q. V. Van, O. Majerus, and L. Hennet, in *Synchrotron Radiation in Materials Science*, edited by R. M. Paniago (2009), Vol. 1092, pp. 71.

10 A. C. Barnes, L. B. Skinner, P. S. Salmon, A. Bytchkov, I. Pozdnyakova, T. O. Farmer, and H. E. Fischer, Physical Review Letters **103** (22) (2009); A. C. Barnes, L. B. Skinner, P. S. Salmon, A. Bytchkov, I. Pozdnyakova, T. O. Farmer, and H. E. Fischer, Physical Review Letters **106** (11) (2011); G. N. Greaves, M. C. Wilding, D. Langstaff, F. Kargl, L. Hennet, C. J. Benmore, J. K. R. Weber, Q. V. Van, O. Majerus, and P. F. McMillan, Journal of Non-Crystalline Solids **357** (2),

435 (2011); M. C. Wilding, G. N. Greaves, Q. V. Van, O. Majerus, and L. Hennet, in *Synchrotron Radiation in Materials Science*, edited by R. M. Paniago (2009), Vol. 1092, pp. 98.

[11] M. Wilson and P. F. McMillan, Physical Review B **69** (5) (2004).

[12] K. Nagashio and K. Kuribayashi, Journal of the American Ceramic Society **85** (9), 2353 (2002); J. K. R. Weber, J. A. Tangeman, T. S. Key, and P. C. Nordine, Journal of Thermophysics and Heat Transfer **17** (2), 182 (2003).

[13] Anthony Bertrand, Julie Carreaud, Gaelle Delaizir, Masato Shimoda, Jean-Rene Duclere, Maggy Colas, Michel Belleil, Julie Comette, Tomokatsu Hayakawa, Cecile Genevois, Emmanuel Veron, Mathieu Allix, Sebastien Chenu, Francois Brisset, and Philippe Thomas, Crystal Growth & Design **15** (10), 5086 (2015).

[14] G. Blasse, G. J. Dirksen, Ewjl Oomen, and M. Tromel, Journal of Solid State Chemistry **63** (2), 148 (1986); M. Tromel, E. Munch, G. Blasse, and G. J. Dirksen, Journal of Solid State Chemistry **76** (2), 345 (1988).

[15] H. G. Burckhardt and M. Tromel, Acta Crystallographica Section C-Crystal Structure Communications **39** (OCT), 1322 (1983).

[16] B. Piriou and H. Arashi, Bulletin De Mineralogie **103** (3-4), 363 (1980).

[17] G. A. Lovas, I. Dodony, L. Poppl, and Z. Szaller, Journal of Solid State Chemistry **135** (2), 175 (1998).

[18] A. P. Hammersley, S. O. Svensson, M. Hanfland, A. N. Fitch, and D. Hausermann, High Pressure Research **14** (4-6), 235 (1996).

[19] Xiangyun Qiu, Jeroen W. Thompson, and Simon J. L. Billinge, Journal of Applied Crystallography **37**, 678 (2004).

[20] D. Waasmaier and A. Kirfel, Acta Crystallographica Section A **51**, 416 (1995).

[21] H. E. Fischer, P. S. Salmon, and A. C. Barnes, Journal De Physique Iv **103**, 359 (2003); H. E. Fischer, A. C. Barnes, and P. S. Salmon, Reports on Progress in Physics **69** (1), 233 (2006).

[22] C. Bernard, V. Keryvin, J. C. Sangleboeuf, and T. Rouxel, Mechanics of Materials **42** (2), 196 (2010); Y. Gueguen, T. Rouxel, P. Gadaud, C. Bernard, V. Keryvin, and J. C. Sangleboeuf, Physical Review B **84** (6) (2011).

[23] N. Saito, N. Hori, K. Nakashima, and K. Mori, Metallurgical and Materials Transactions B-Process Metallurgy and Materials Processing Science **34** (5), 509 (2003).

[24] Y. L. Wang, S. X. Dai, F. F. Chen, T. F. Xu, and Q. H. Nie, Materials Chemistry and Physics **113** (1), 407 (2009).

[25] S. Susman, K. J. Volin, D. L. Price, M. Grimsditch, J. P. Rino, R. K. Kalia, P. Vashishta, G. Gwanmesia, Y. Wang, and R. C. Liebermann, Physical Review B **43** (1), 1194 (1991); S. Susman, K. J. Volin, D. G. Montague, and D. L. Price, Physical Review B **43** (13), 11076 (1991).

[26] P. S. Salmon, Nature Materials **1** (2), 87 (2002); P. S. Salmon, R. A. Martin, P. E. Mason, and G. J. Cuello, Nature **435** (7038), 75 (2005); P. S. Salmon, A. C. Barnes, R. A. Martin, and G. J. Cuello, Physical Review Letters **96** (23) (2006).

[27] N. E. Brese and M. Okeeffe, Acta Crystallographica Section B-Structural Science **47**, 192 (1991); M. Okeeffe and N. E. Brese, Acta Crystallographica Section B-Structural Science **48**, 152 (1992).

[28] A. C. Hannon and J. M. Parker, Journal of Non-Crystalline Solids **274** (1-3), 102 (2000).

[29] J. Lin, W. Huang, L. Ma, Q. Bian, S. Qin, H. Wei, and J. Chen, Materials Science-Poland **27** (1), 329 (2009); Hooi Ming Oo, Halimah Mohamed-Kamari, and Wan Mohd Daud Wan-Yusoff, International Journal of Molecular Sciences **13** (4), 4623 (2012).

[30] J. C. McLaughlin and J. W. Zwanziger, Journal of Molecular Graphics & Modelling **17** (5-6), 275 (1999).

[31] J. C. McLaughlin, S. L. Tagg, J. W. Zwanziger, D. R. Haeffner, and S. D. Shastri, Journal of Non-Crystalline Solids **274** (1-3), 1 (2000).

[32] Volker L. Deringer, Ralf P. Stoffel, and Richard Dronskowski, Crystal Growth & Design **14** (2), 871 (2014); Ralf P. Stoffel, Volker L. Deringer, Ronnie E. Simon, Raphael P. Hermann, and Richard Dronskowski, Journal of Physics-Condensed Matter **27** (8) (2015).

[33] J. C. McLaughlin, S. L. Tagg, and J. W. Zwanziger, Journal of Physical Chemistry B **105** (1), 67 (2001); J. W. Zwanziger, J. C. McLaughlin, and S. L. Tagg, in *Structure and Dynamics of Glasses and Glass Formers*, edited by C. A. Angell, K. L. Ngai, J. Kieffer et al. (1997), Vol. 455, pp. 405; J. W. Zwanziger, J. C. McLaughlin, and S. L. Tagg, Physical Review B **56** (9), 5243 (1997).

[34] R. Akagi, K. Handa, N. Ohtori, A. C. Hannon, M. Tatsumisago, and N. Umesaki, Journal of Non-Crystalline Solids **256**, 111 (1999); R. Akagi, K. Handa, N. Ohtori, A. C. Hannon, M. Tatsumisago, and N. Umesaki, Japanese Journal of Applied Physics Part 1-Regular Papers Short Notes & Review Papers **38**, 160 (1999); Emma R. Barney, Alex C. Hannon, Diane Holland, Norimasa Umesaki, Masahiro Tatsumisago, Robin G. Orman, and Steve Feller, Journal of Physical Chemistry Letters **4** (14), 2312 (2013); Emma R. Barney, Alex C. Hannon, Diane Holland, Norimasa Umesaki, and Masahiro Tatsurnisago, Journal of Non-Crystalline Solids **414**, 33 (2015).

[35] P. Veber and J. Mangin, Materials Research Bulletin **43** (11), 3066 (2008).

[36] C. A. Angell, Science **267** (5206), 1924 (1995).

[37] D. M. Zhu, C. S. Ray, W. C. Zhou, and D. E. Day, Journal of Non-Crystalline Solids **319** (3), 247 (2003).

[38] M. C. Wilding, P. F. McMillan, and A. Navrotsky, Physics and Chemistry of Glasses **43** (6), 306 (2002).

Figure

(a)

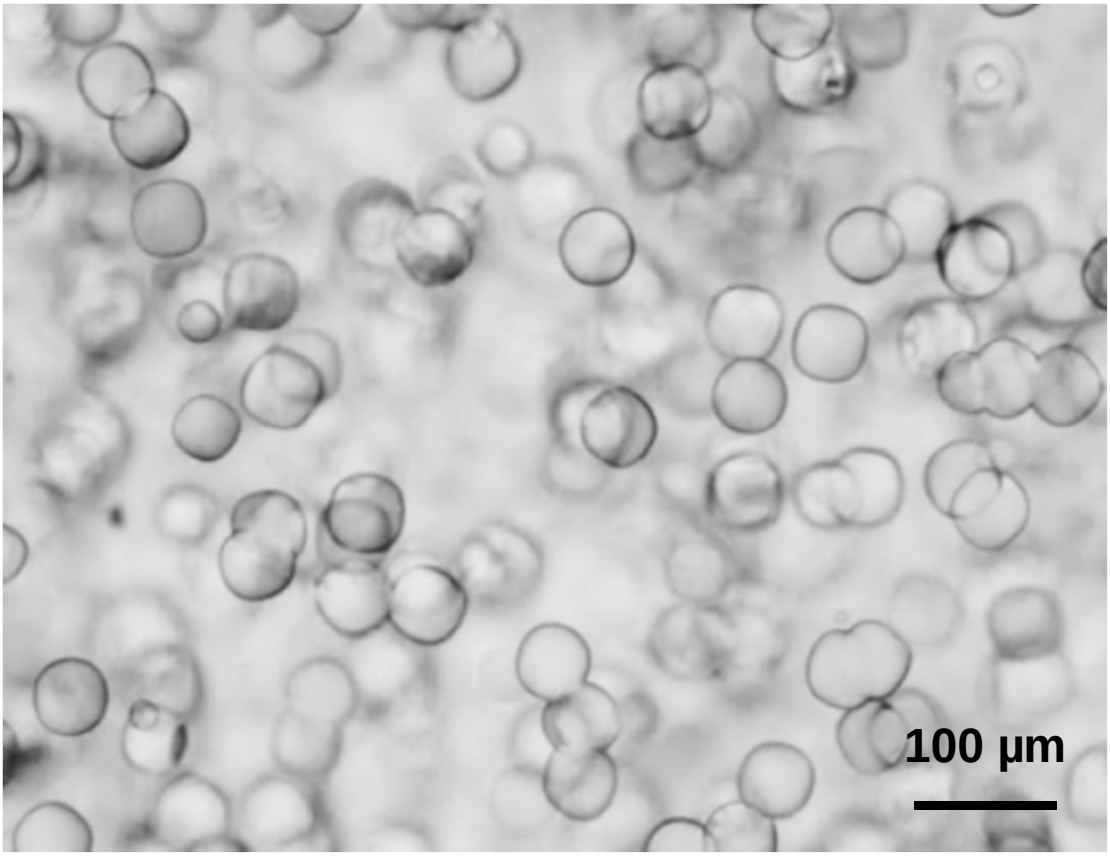

(b)

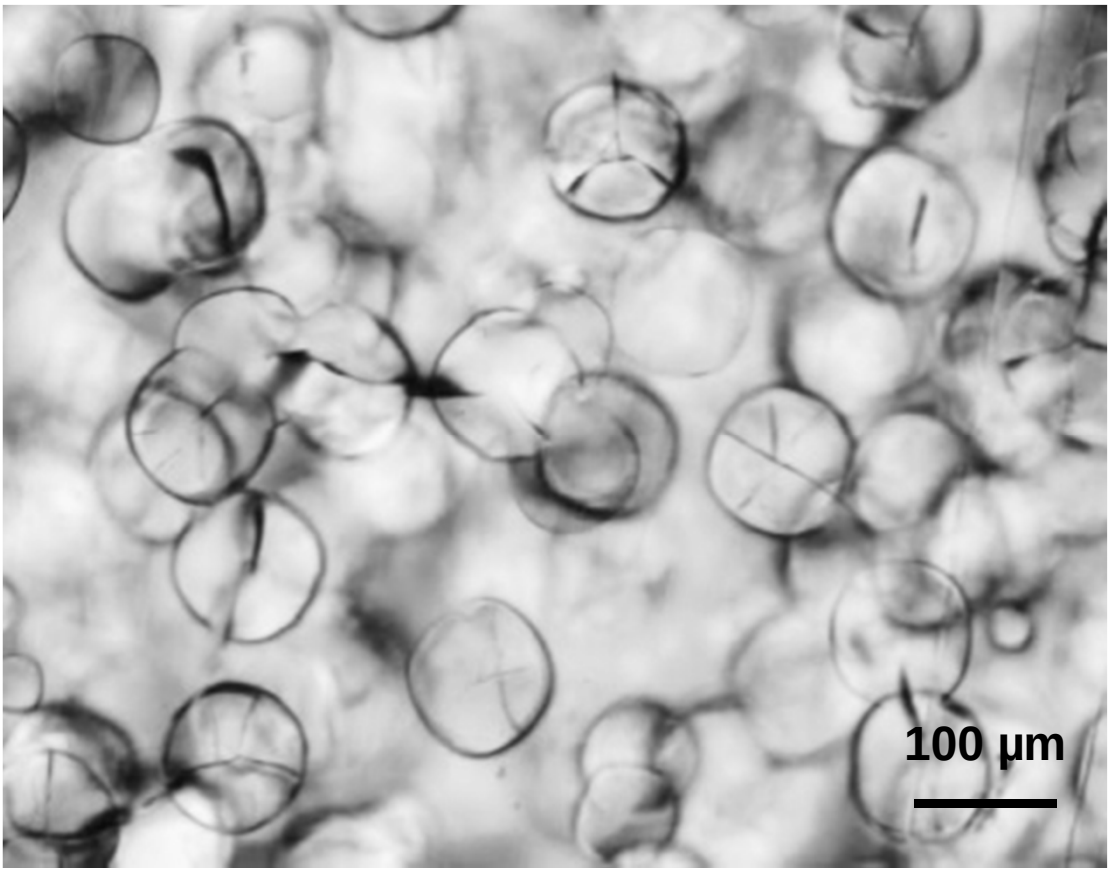

Figure

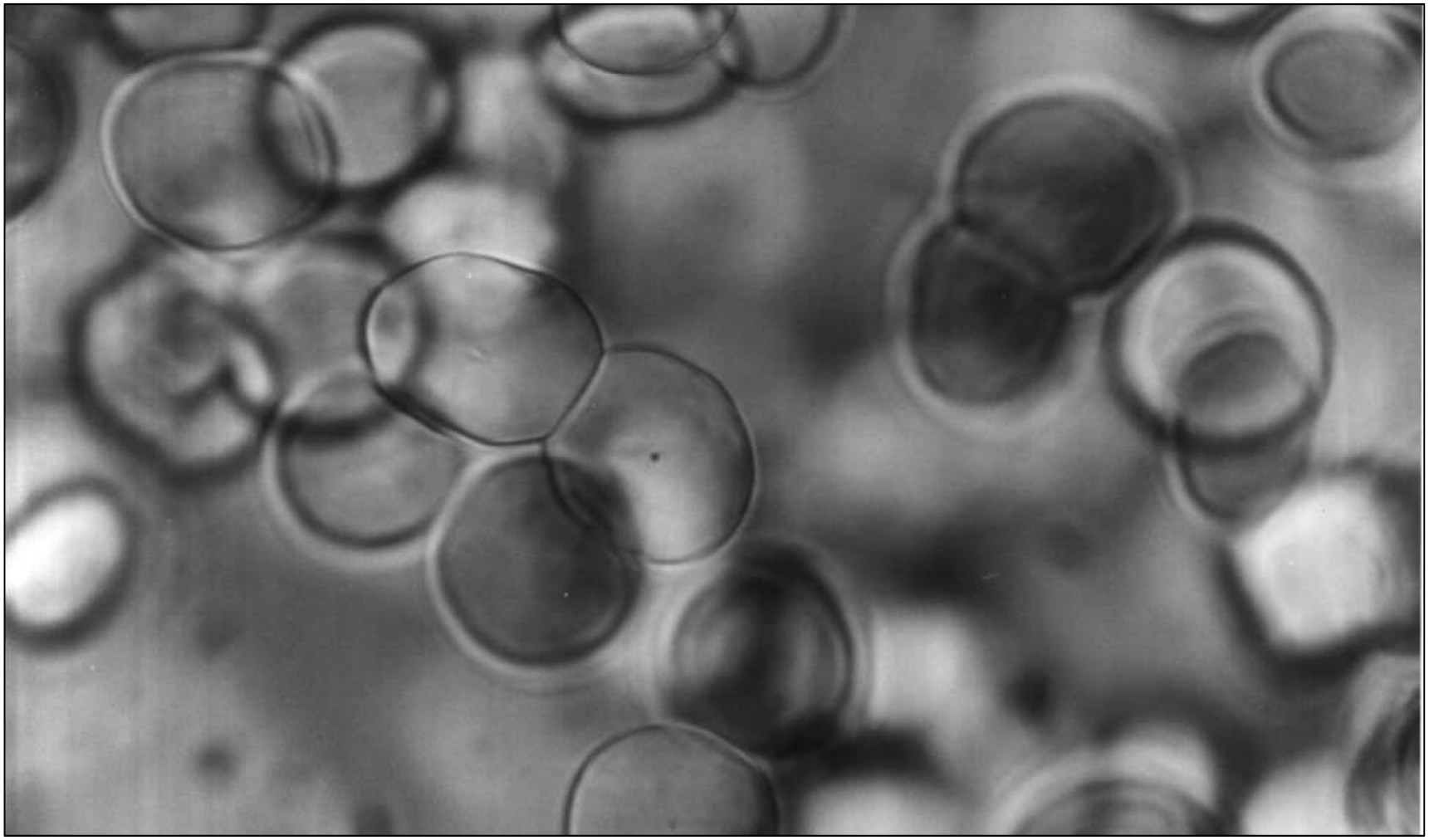

Figure

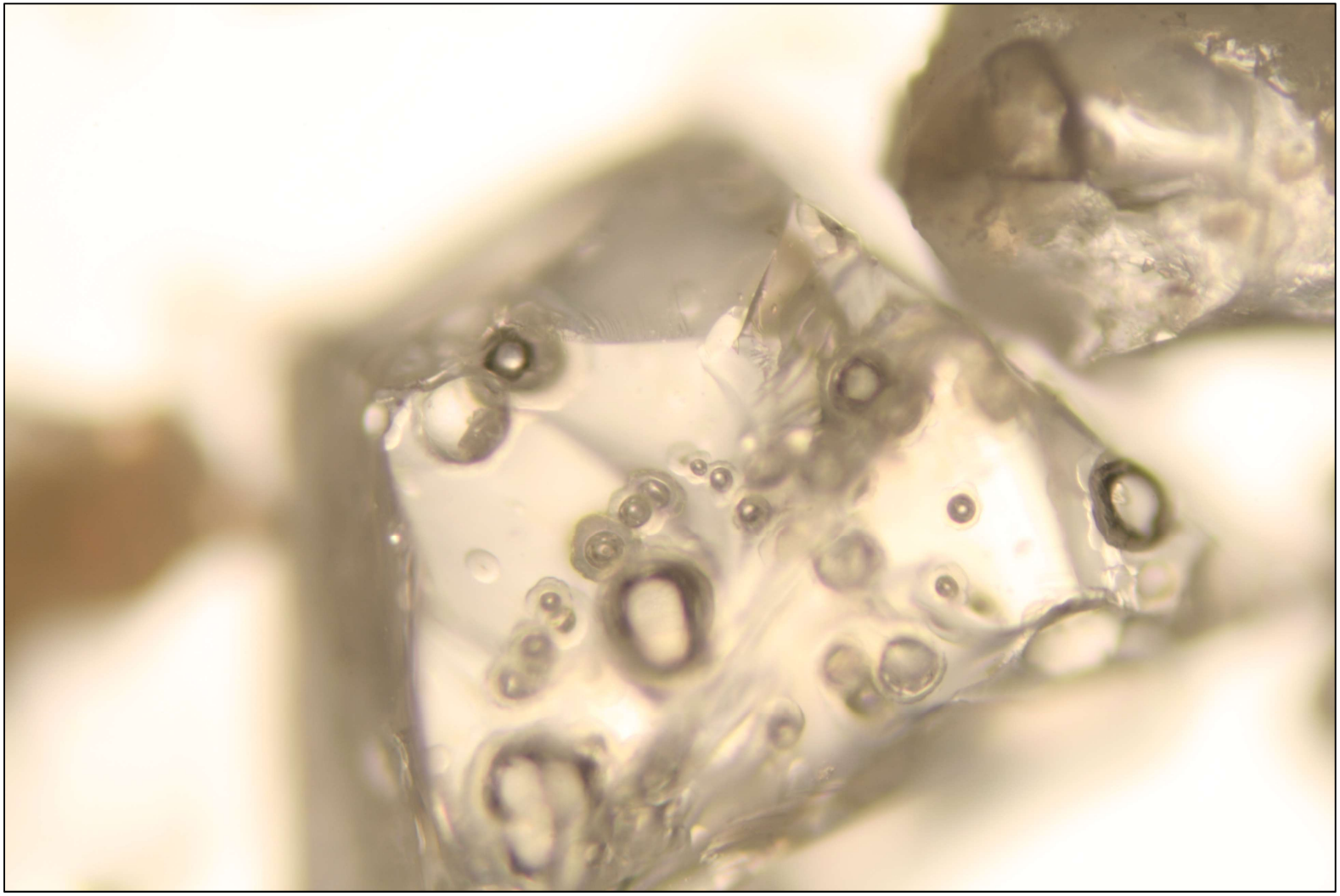

Figure

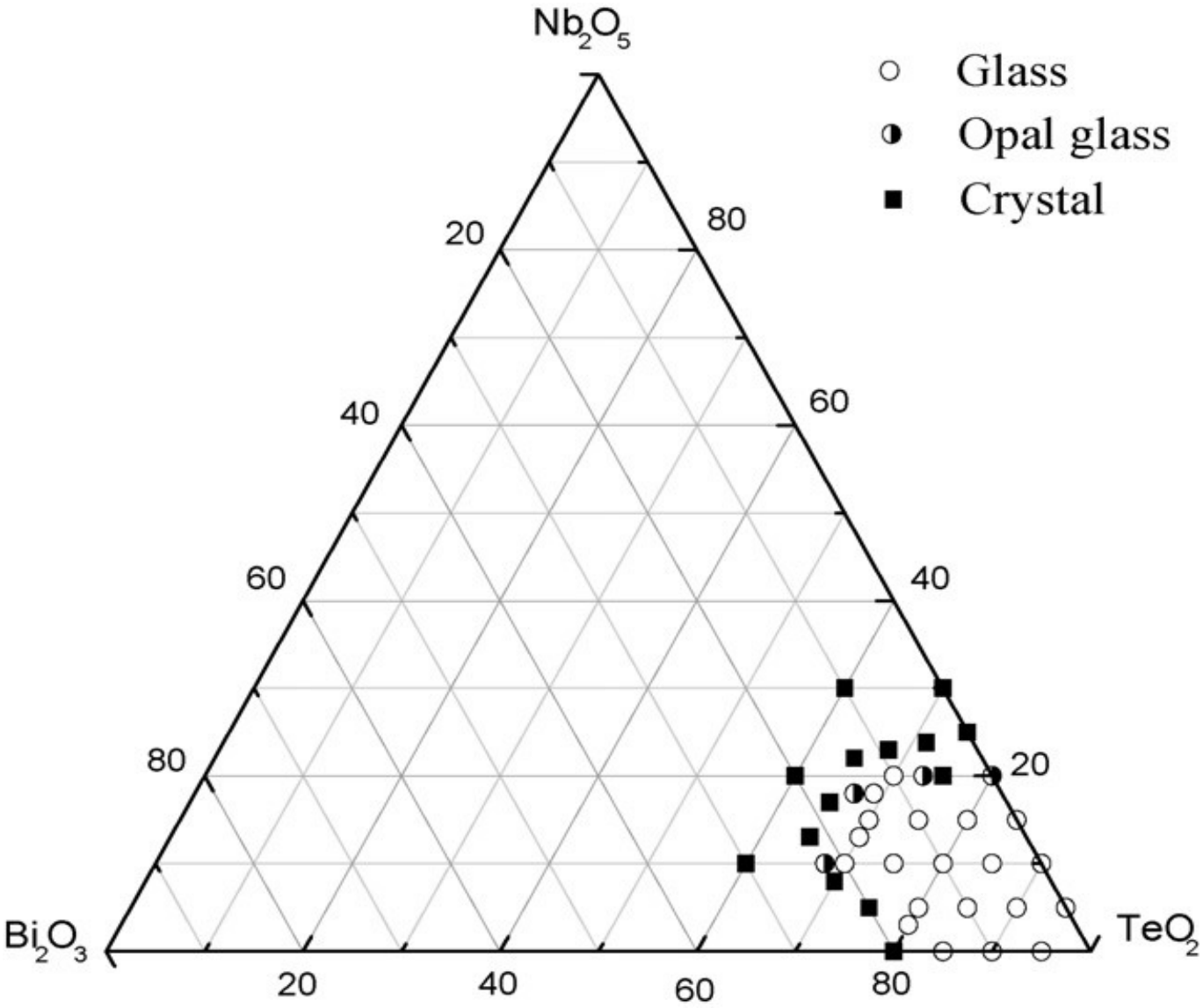
Nb2O5
Glass
Opal glass
Crystal
20
40
60
80
80
60
40
20
Bi2O3
20
40
60
80
TeO2

Figure

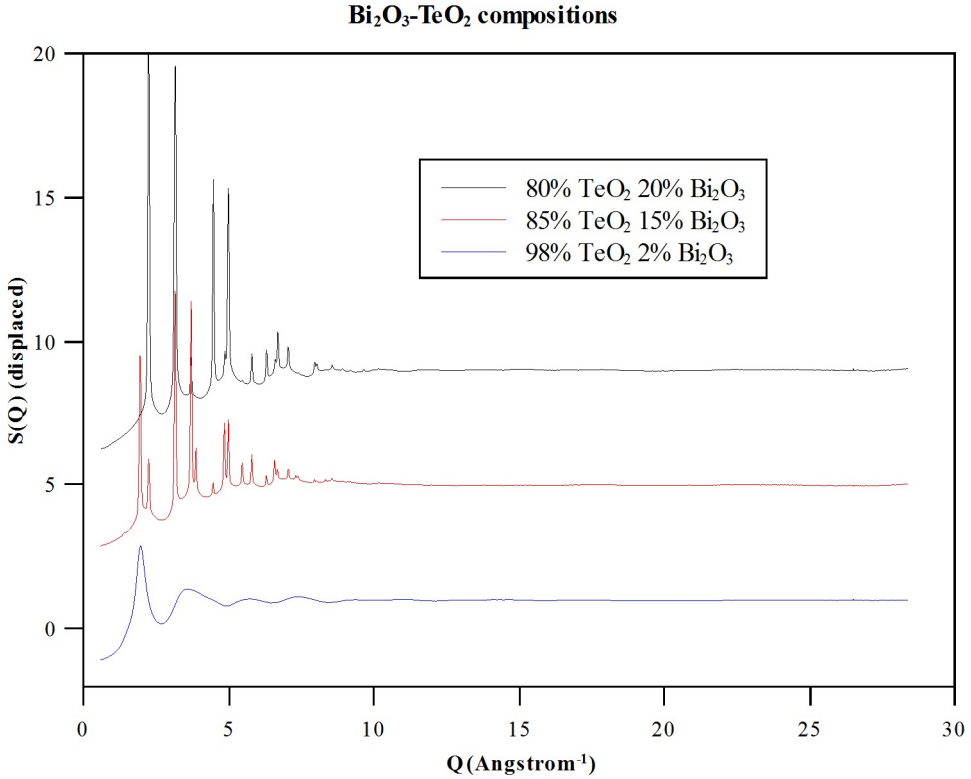
Bi2O3-TeO2 compositions
80% TeO2 20% Bi2O3
85% TeO2 15% Bi2O3
98% TeO2 2% Bi2O3
S(Q) (displaced)
Q(Angstrom-1)
0
5
10
15
20
25
30

Figure

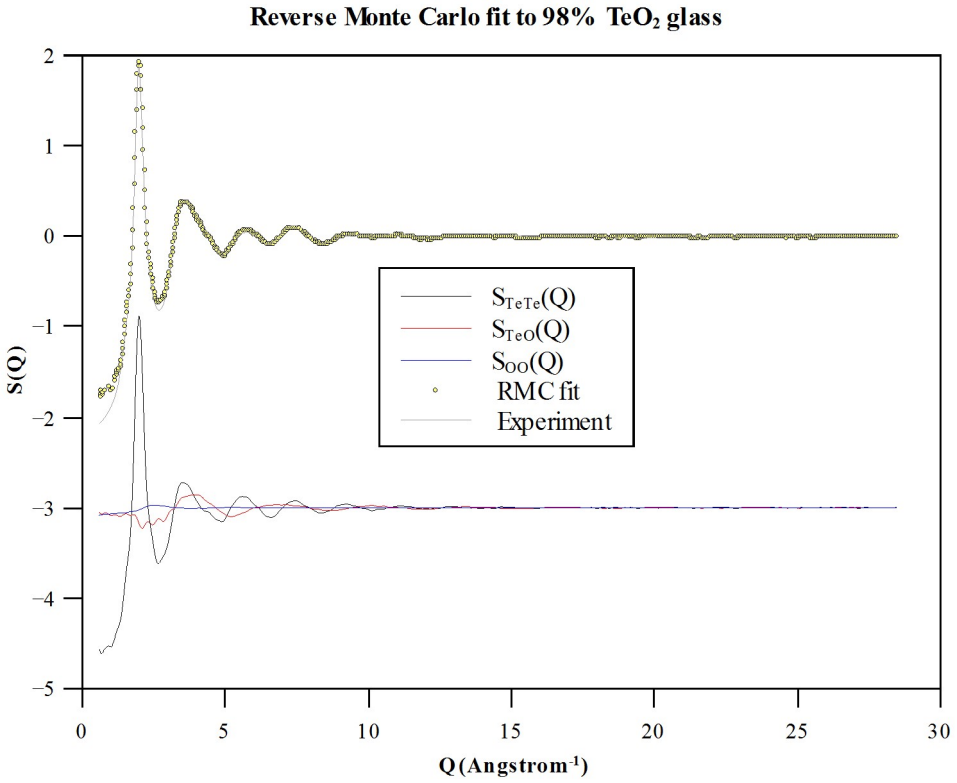
Reverse Monte Carlo fit to 98% TeO2 glass
S(Q)
Q (Angstrom-1)
STeTe(Q)
STeO(Q)
SOO(Q)
RMC fit
Experiment
2
1
0
−1
−2
−3
−4
−5
0
5
10
15
20
25
30

Figure

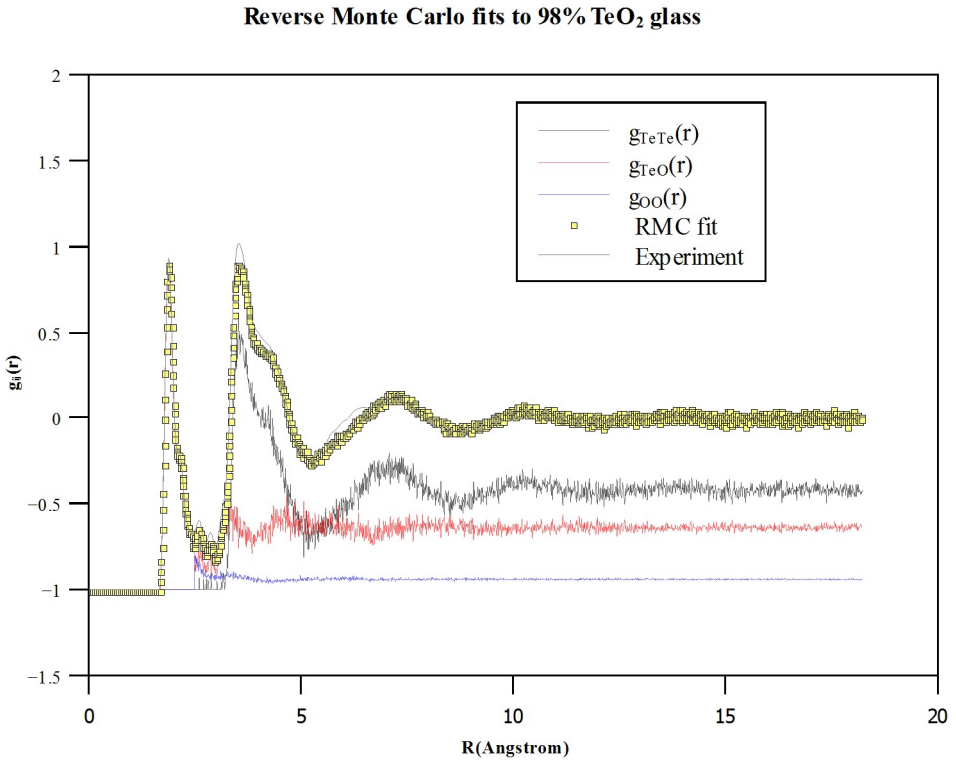
Reverse Monte Carlo fits to 98% TeO2 glass
gTeTe(r)
gTeO(r)
gOO(r)
RMC fit
Experiment
gij(r)
R(Angstrom)
2
1.5
1
0.5
0
−0.5
−1
−1.5
0
5
10
15
20

Figure

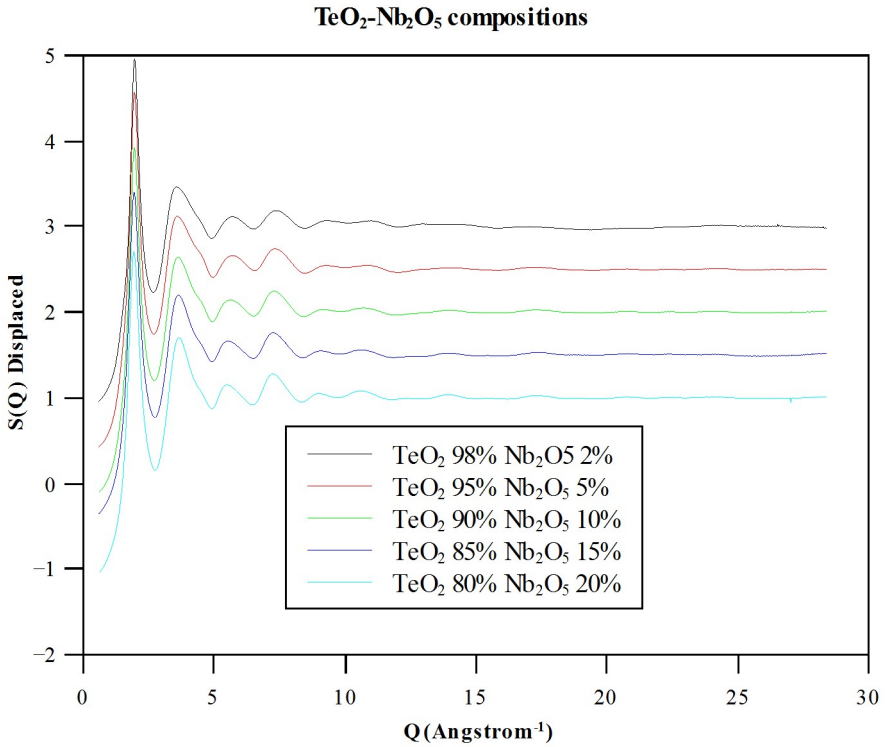
TeO2-Nb2O5 compositions
S(Q) Displaced
Q(Angstrom-1)
TeO2 98% Nb2O5 2%
TeO2 95% Nb2O5 5%
TeO2 90% Nb2O5 10%
TeO2 85% Nb2O5 15%
TeO2 80% Nb2O5 20%
5
4
3
2
1
0
−1
−2
0
5
10
15
20
25
30

Figure

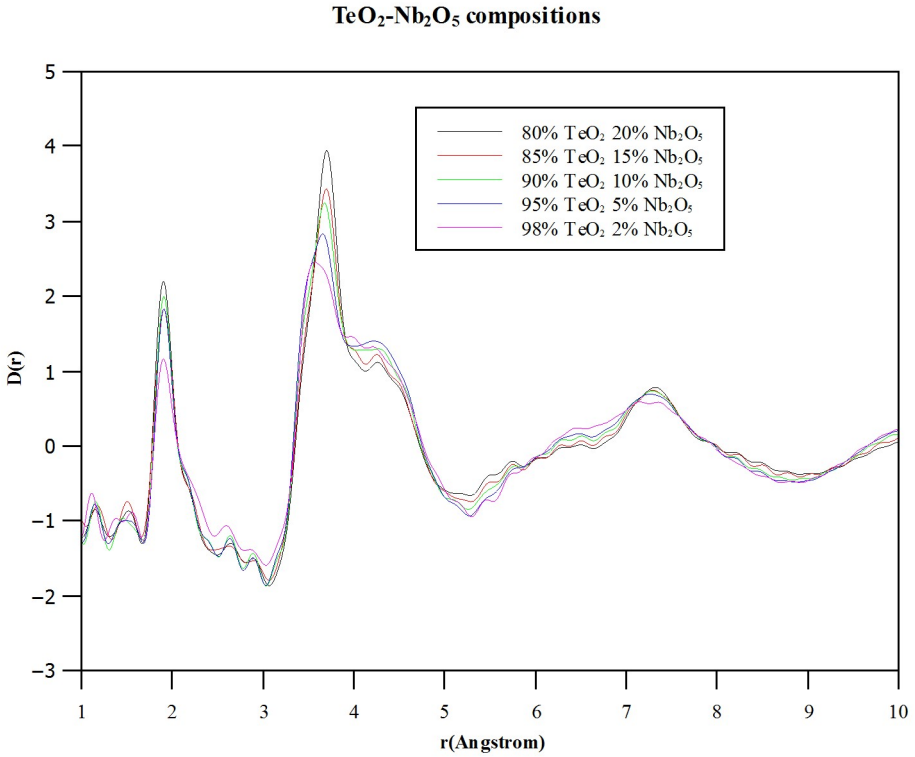
TeO2-Nb2O5 compositions
80% TeO2 20% Nb2O5
85% TeO2 15% Nb2O5
90% TeO2 10% Nb2O5
95% TeO2 5% Nb2O5
98% TeO2 2% Nb2O5
D(r)
r(Angstrom)
5
4
3
2
1
0
−1
−2
−3
1
2
3
4
5
6
7
8
9
10

Figure

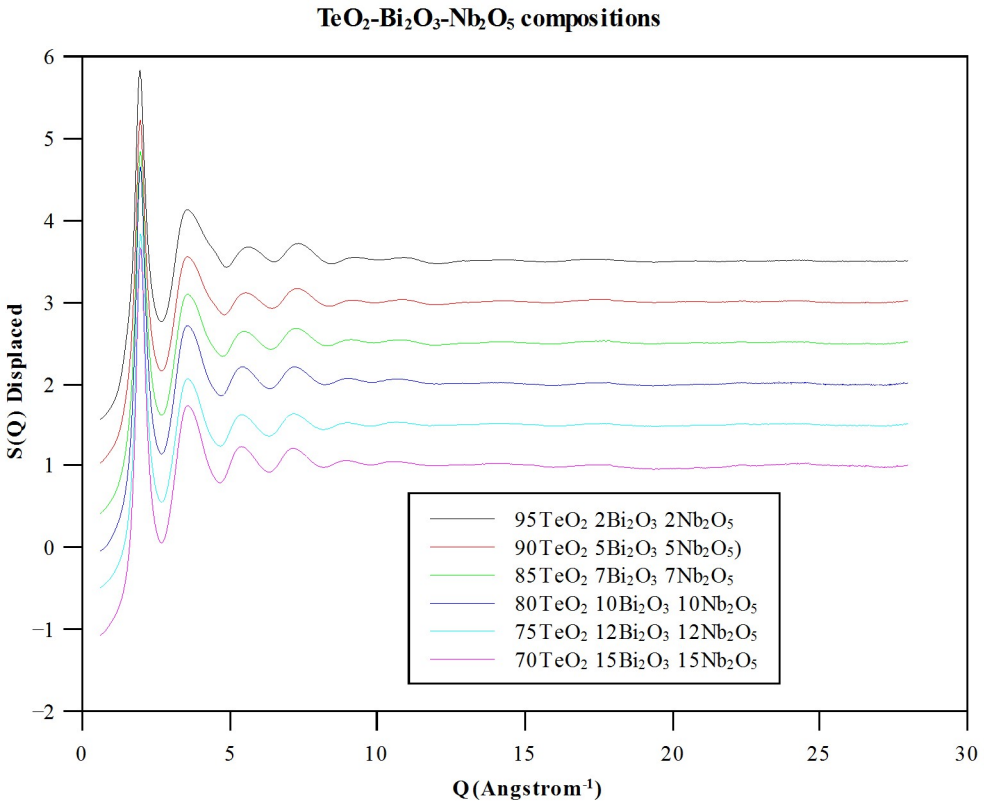
TeO2-Bi2O3-Nb2O5 compositions
S(Q) Displaced
Q (Angstrom-1)
95TeO2 2Bi2O3 2Nb2O5
90TeO2 5Bi2O3 5Nb2O5)
85TeO2 7Bi2O3 7Nb2O5
80TeO2 10Bi2O3 10Nb2O5
75TeO2 12Bi2O3 12Nb2O5
70TeO2 15Bi2O3 15Nb2O5

Figure

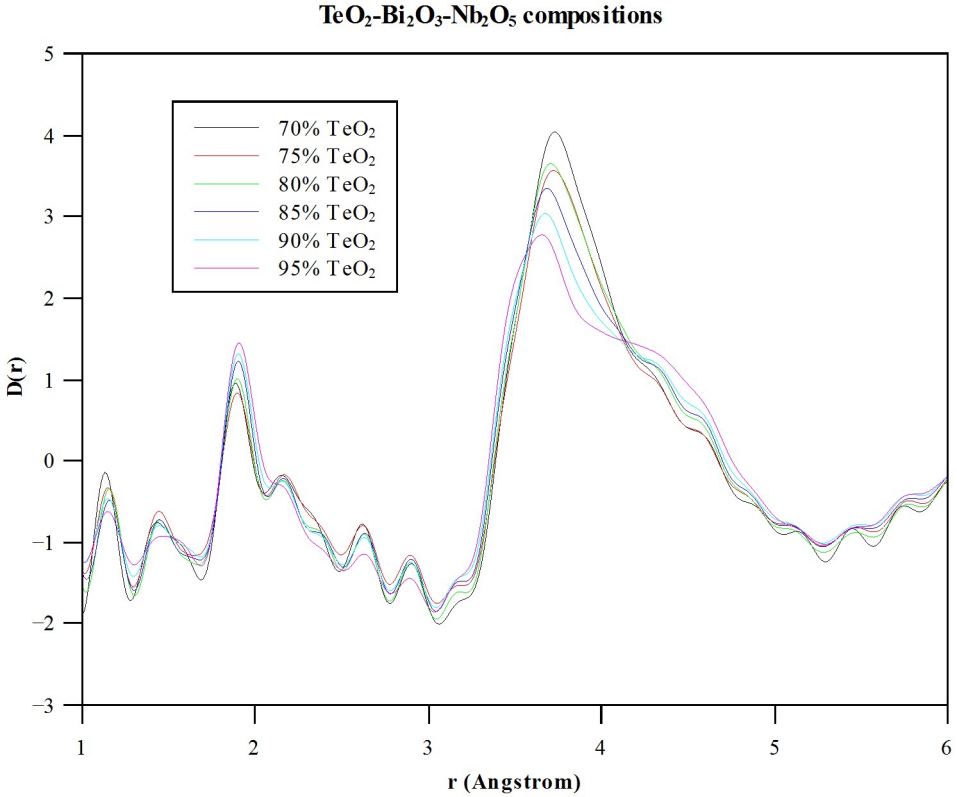
TeO2-Bi2O3-Nb2O5 compositions
70% TeO2
75% TeO2
80% TeO2
85% TeO2
90% TeO2
95% TeO2
D(r)
r (Angstrom)
5
4
3
2
1
0
−1
−2
−3
1
2
3
4
5
6

Figure

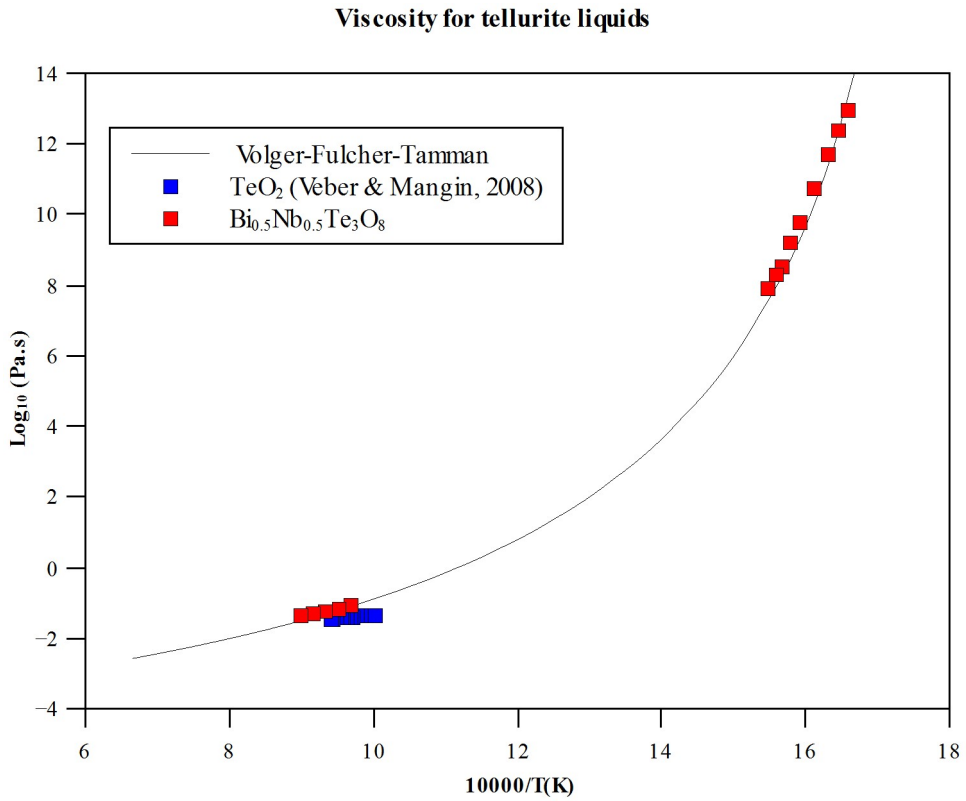
Viscosity for tellurite liquids
Volger-Fulcher-Tamman
TeO2 (Veber & Mangin, 2008)
Bi0.5Nb0.5Te3O8
Log10 (Pa.s)
10000/T(K)
14
12
10
8
6
4
2
0
−2
−4
6
8
10
12
14
16
18